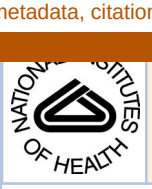

Published in final edited form as:

Cell. 2013 September 26; 155(1): 188–199. doi:10.1016/j.cell.2013.09.004.

Mitochondrial dynamics controlled by mitofusins regulate Agrp neuronal activity and diet-induced obesity

Marcelo O. Dietrich[1,2], **Zhong-Wu Liu**[1], and **Tamas L. Horvath**[1]

[1]Program in Integrative Cell Signaling and Neurobiology of Metabolism, Section of Comparative Medicine, Yale University School of Medicine, New Haven, CT - 06520 - USA

[2]Department of Biochemistry, Universidade Federal do Rio Grande do Sul, Porto Alegre, RS - 90035 - Brazil

Summary

Mitochondria are key organelles in the maintenance of cellular energy metabolism and integrity. Here we show that mitochondria number decrease but their size increase in orexigenic Agrp neurons during the transition from fasted to fed to over-fed state. These fusion-like dynamic changes were cell-type specific, as they occurred in the opposite direction in anorexigenic POMC neurons. Interfering with mitochondrial fusion mechanisms in Agrp neurons by cell-selectively knocking down mitofusin-1 (Mfn1) or mitofusin-2 (Mfn2) resulted in altered mitochondria size and density in these cells. Deficiency in mitofusins impaired the electric activity of Agrp neurons during high-fat diet, an event reversed by cell-selective administration of ATP. Agrp-specific Mfn1 or Mfn2 knockout mice gained less weight when fed a high-fat diet due to decreased fat mass. Overall, our data unmask an important role for mitochondrial dynamics governed by Mfn1 and Mfn2 in Agrp neurons in central regulation of whole body energy metabolism.

Introduction

Maintenance of energy metabolism is a fundamental homeostatic function to sustain life from single cells to complex organisms. In eukaryotes, mitochondria are key organelles that allow efficient energy production through the respiratory chain to sustain biological reactions. Mitochondria are complex organelles organized in intricate intracellular networks. Highly dynamic, these organelles respond to changes in the cellular environment and adapt their morphology and location to optimize cell function. As early as 1914, dynamic changes in mitochondria shape and distribution were described (Lewis and Lewis, 1914). More recently, it was shown that mitochondria shape, morphology and number are tightly regulated by the processes of fusion and fission (Cerveny et al., 2007). Numerous molecules have been discovered to participate in these processes, with mitofusins (Mfn1 and Mfn2)

Correspondence to: tamas.horvath@yale.edu or marcelo.dietrich@yale.edu.

(Chen et al., 2003; Eura et al., 2003; Ishihara et al., 2004; Rojo et al., 2002; Santel and Fuller, 2001) and optic atrophy-1 (OPA1) (Cipolat et al., 2004; Song et al., 2009) as main players to drive fusion, and dynamin-related protein-1 (Drp1) leading to fission (Reddy et al., 2011; Smirnova et al., 1998).

Complex organisms must also coordinate whole body energy balance with that of cellular energetics. In mammals, the hypothalamus located in the basal part of the brain plays a critical role in orchestrating whole body energy homeostasis (Dietrich and Horvath, 2009). More specifically, a subset of neurons located in the arcuate nucleus of the hypothalamus that produces agouti-related peptide (Agrp) and neuropeptide-Y (NPY) (Broberger et al., 1998; Horvath et al., 1997; Ollmann et al., 1997) exerts a fundamental role in the promotion of feeding (Chen et al., 2004; Clark et al., 1984; Zarjevski et al., 1993). The NPY/Agrp neurons (thereof Agrp neurons) are special in that their activity must be at the highest level, when the whole body is lacking sufficient energy, such as food deprivation or fasting (Hahn et al., 1998; Kohno et al., 2008; Sternson et al., 2005; Takahashi and Cone, 2005; Yang et al., 2011). Located in the vicinity of Agrp neurons, there is another population of cells that produce pro-opiomelanocortin (POMC neurons) and exert an opposite function (Aponte et al., 2011; Cone, 2005). Because mitochondria-related genes have been tied to Agrp neurons and their functioning (Andrews et al., 2008; Coppola et al., 2007; Horvath et al., 1999), here we analyzed mitochondria dynamics in orexigenic Agrp neurons during various metabolic states and assessed the role of Mfn1 and Mfn2 in these processes.

Results

Mitochondria in Agrp neurons

Mitochondria fusion and fission are the two main processes involved in mitochondria dynamics (Figure 1A) (Cerveny et al., 2007). The proteins involved in such processes, as for example mitofusins (Eura et al., 2003), are broadly expressed throughout mammalian tissues (Rojo et al., 2002; Santel et al., 2003). To study mitochondria changes in Agrp neurons, we used electron microscopy to identify single cells and analyze mitochondria shape and morphology (Figure 1B, C). In NPY-tau-sapphireFP mice (Pinto et al., 2004), Agrp neurons (Figure 1B) contain numerous elliptical mitochondria, slightly elongated (Figure 1C), similarly to the neighbors POMC cells (Schneeberger et al., 2013). We observed mitochondria tethering in Agrp neurons (Figure 1A, D), whereby the outer membranes of mitochondria are in contact in a process dependent of numerous protein complexes, including mitofusins (Chen et al., 2003; Ishihara et al., 2004; Rojo et al., 2002). We also detected fusion of the outer membranes of mitochondria in Agrp neurons (Figure 1E). We confirmed the presence of transcripts of genes involved in mitochondria fusion-fission in Agrp neurons utilizing individual cell capture real-time PCR (Figure 1F). These included *mfn1*, *mfn2*, and *opa1*, involved in mitochondria fusion; also, we detected expression of *drp1*, involved in fission (Figure 1F).

Metabolic status modifies mitochondria in Agrp neurons

To analyze the effect of metabolic status on mitochondria of Agrp neurons, first, we analyzed the response of these neurons to food deprivation. Twenty-four hours food

deprivation increased mitochondria density in Agrp neurons (Figure 2A) (Coppola et al., 2007), but not mitochondria coverage of the cellular (data not shown) or cytosolic areas (Figure 2B). The increase in mitochondria number (Figure 2A) was accompanied by a decrease in mitochondria size (Figure 2C). The shape of mitochondria in the Agrp neurons was not changed after food deprivation (Figure 2D). Thus, these data indicate that food deprivation leads to an increase in mitochondria density and a decrease in mitochondria size in Agrp neurons, which is characteristic of changes in mitochondria dynamics towards fission (Figure 2I, K). The effect of food deprivation on mitochondria dynamics appears to be cell population-specific, as other neuronal cells showed different response. Neighboring, anorexigenic POMC cells presented a decrease in mitochondria density and coverage, without changes in mitochondria morphology (Figure S1).

Next, we determined whether high-fat feeding impacts mitochondria dynamics in Agrp neurons. Even though mice fed a high-fat diet (HFD) have decreased levels of *npy* and *agrp* mRNA in the arcuate nucleus (data not shown) (Horvath et al., 2010), we found that Agrp neurons are highly active under these conditions as assessed by electrophysiology (Diano et al., 2011), and they exert a stronger inhibitory tone on POMC neurons compared to normal chow fed mice (Newton et al., 2012). High-fat feeding decreased mitochondria density (Figure 2E) and coverage (Figure 2F) in Agrp neurons. These changes occurred concurrently with significant increases in mitochondria size (Figure 2G) and elongation (Figure 2H). The constellation of modifications in mitochondria morphology and density that occurred after high fat feeding in the Agrp neurons is indicative of increased fusion under such metabolic conditions (Figure 2J, K). Again, these changes were cell-type specific because they did not occur in POMC neurons (data not shown) (Diano et al., 2011; Schneeberger et al., 2013). Taken together these observations suggest that food deprivation leads to mitochondria fission while high-fat feeding leads to mitochondria fusion in Agrp neurons (Figure 2K).

Mitofusins in Agrp neurons regulate mitochondria shape and size

Using cell-specific ribosome profiling (Sanz et al., 2009), we analyzed the levels of *mfn1* and *mfn2* mRNA bound to ribosomes in Agrp neurons from fed, fasted and high-fat diet fed mice. We were unable to find significant differences in these transcripts among the groups analyzed (Figure S2). To further interrogate the role of mitofusins in the cellular changes that occur in the Agrp neurons, we generated mice that lacked Mfn1 or Mfn2 in these cells (Agrp-Mfn1$^{-/-}$ and Agrp-Mfn2$^{-/-}$ mice).

Agrp neurons from Agrp-Mfn1$^{-/-}$ mice did not present major changes in mitochondria parameters under normal chow diet conditions (Figure 3A–C), besides a decrease in mitochondria aspect ratio (Figure 3D, I), which indicates a more rounded shape of mitochondria in the Mfn1$^{-/-}$ cells. In Agrp-Mfn2$^{-/-}$ mice, the number of mitochondria was unaltered (Figure 3E), even though there was an increase in mitochondria coverage of cellular and cytosolic compartments (Figure 3F). This increase in coverage was due to an increase in mitochondria size in Mfn2$^{-/-}$ neurons (Figure 3G, J). The changes in size were not accompanied by changes in shape (Figure 3H, J). Thus, lack of Mfn1 in the Agrp neurons led to changes in mitochondria shape, while lack of Mfn2 led to changes in mitochondria size.

Lack of mitofusins does not lead to Agrp neuronal degeneration or altered projections

In some cells types, knockdown of mitofusin proteins led to neuronal cell death (Jahani-Asl et al., 2007). We counted the number of Agrp neurons in the arcuate nucleus from littermate control mice and Agrp-Mfn1$^{-/-}$ or Agrp-Mfn2$^{-/-}$ adult mice and we did not find any evidence of neuronal cell death (data not shown). We also did not find any changes in nuclear and cell sizes (data not shown). We did not find changes in gene expression for *npy*, *agrp* and *pomc* in the hypothalamus of Agrp-Mfn1$^{-/-}$ and Agrp-Mfn2$^{-/-}$ mice (Figure S5). We measured Agrp neuronal projections in control and Agrp-Mfn1$^{-/-}$/Agrp-Mfn2$^{-/-}$ mice, and we did not find any statistical difference between these groups of mice (Figure S3). Importantly, the intensity of Agrp staining on fiber terminals did not differ between groups, indicating that the content of neuropeptides in Agrp-Mfn1$^{-/-}$/Agrp-Mfn2$^{-/-}$ neurons was intact (Figure S3).

Because Mfn2 has also been related to mitochondria-ER interactions, and not only mitochondria-mitochondria fusion, we measured the amount of contacts between mitochondria and ER in control and Mfn2$^{-/-}$ neurons. We did not find any differences in mitochondria-ER connections (control = 1.00 ± 0.07, n = 50; Mfn2$^{-/-}$ = 0.96 ± 0.09, n = 23; relative units – $t_{71} = 0.25$, $P > 0.05$) suggesting Mfn2 in Agrp neurons does not play a critical role in this organelle interaction. Because knockout of Mfn2 in POMC neurons in the hypothalamus leads to hypothalamic ER stress (Schneeberger et al., 2013), we analyzed ER stress related genes in the hypothalami of control and Agrp-Mfn2$^{-/-}$ mice, and we found no significant differences (Figure S3). These findings are in agreement with the lack of morphological evidences of ER stress in Agrp-Mfn2$^{-/-}$ cells (Figure 3J). We also analyzed the expression of ER stress related genes in Agrp-Mfn1$^{-/-}$ mice, and we found no differences compared to control mice (Figure S3).

Mfn1 and Mfn2 deletion in Agrp neurons impairs cellular response to a HFD

Next, we determined whether Agrp-Mfn1$^{-/-}$/Agrp-Mfn2$^{-/-}$ mice have altered cellular and metabolic responses to a HFD. Agrp-Mfn1$^{-/-}$ and Mfn2$^{-/-}$ neurons from mice fed a HFD had increase mitochondria number (Figure 4A, E) and mitochondria coverage (Figure 4B, F) when compared to neurons from control mice fed the same diet. While Agrp-Mfn1$^{-/-}$ neurons show mitochondria of similar size (Figure 4C) but less elongated (Figure 4D) compared to HFD fed control mice, Agrp-Mfn2$^{-/-}$ neurons had mitochondria of decreased size (Figure 4G), but with similar shape (Figure 4H). It is important to note that wild-type mice fed a HFD have increased mitochondria size accompanied by decreased mitochondria density in the Agrp neurons (Figure 2). Both Agrp-Mfn1$^{-/-}$ and Agrp-Mfn2$^{-/-}$ neurons did not present decreases in mitochondria density in response to HFD indicating a critical role for these proteins in HFD-induced decreases in mitochondria density in Agrp neurons. Mfn1 was also involved in changes in mitochondria shape (Figure 4D), whereas Mfn2 was critical for changes in mitochondria size that occurs during HFD (Figure 4G), an effect similar to what we observed in normal chow fed mice (Figure 3). Overall, the constellation of changes that occur in Agrp neuronal mitochondria during high-fat feeding was dependent, at least in part, of the expression of both Mfn1 and Mfn2.

Similarly to what we found in Agrp-Mfn1$^{-/-}$/Agrp-Mfn2$^{-/-}$ mice fed a regular chow diet, mice fed a HFD also did not present any changes in the Agrp fiber density in the PVN (data not shown) and in the number of Agrp neurons in the arcuate nucleus (data not shown). These data indicate that in both normal chow and HFD conditions, there is no neuronal loss in Agrp-Mfn1$^{-/-}$/Agrp-Mfn2$^{-/-}$ cells. In addition, we also quantified the levels of *agrp*, *npy* and *pomc* mRNA in the arcuate nucleus from these mice fed a HFD. While we found no differences in the levels of *agrp* and *npy*, we found a significant decrease in *pomc* levels in Agrp-Mfn2$^{-/-}$ compared to control mice (Figure S3). Agrp-Mfn1$^{-/-}$ mice show no differences in the levels of these transcripts compared to control mice (Figure S3). Similarly to normal chow fed mice, we did not find any differences in mitochondria-ER connections between control and Agrp-Mfn2$^{-/-}$ neurons (control = 1.00 ± 0.06, n = 30; Mfn2$^{-/-}$ = 0.86 ± 0.08, n = 30; relative units – t_{58} = 1.407, P > 0.05). Gene expression analyzes of ER-stress related genes in the hypothalamus of either Agrp-specific Mfn1 or Mfn2 knockout mice fed a HFD did not show differences between groups (Figure S3). This set of data emphasizes the lack of effect of Agrp-specific mitofusins knockout in the propagation of ER-stress in the hypothalamus, contrary to what was observed in POMC-specific Mfn2$^{-/-}$ mice (Schneeberger et al., 2013).

Mfn1 and Mfn2 regulate the electric activity of Agrp neurons during HFD

Next, we sought to determine whether Mfn1 and/or Mfn2 impact the electrical properties of Agrp neurons. Using patch-clamp electrophysiology recording, we measured the action potential frequency of these neurons in mice fed a normal chow or a HFD. Under normal chow diet, we did not find statistical differences in the mean firing rate of Agrp neurons from control and Agrp-Mfn1$^{-/-}$/Agrp-Mfn2$^{-/-}$ mice (Figure 5A, E). When mice were fed a HFD, Agrp neurons from both Agrp-specific knockout mice presented decreased firing rate when compared to Agrp neurons from littermate control mice (Figure 5B, F). Notably, in control mice high-fat feeding decreased the number of silent Agrp neurons (normal chow = 22.09 % silent (19 in 86 cells), HFD = 8.42 % silent (8 in 95 cells); P = 0.012, Fisher's exact test). This adaptation in the electrical properties of Agrp neurons in response to high-fat feeding was abolished in Agrp-Mfn1$^{-/-}$ (Figure 5C–D) and Agrp-Mfn2$^{-/-}$ (Figure 5G–H) neurons, which showed an increase in number of silent Agrp neurons when mice were fed a HFD.

Equalizing intracellular ATP level rescues electrical properties of Agrp-Mfn1$^{-/-}$ and Mfn2$^{-/-}$ neurons

One possibility to explain the decrease in electrical activity of Mfn1$^{-/-}$/Mfn2$^{-/-}$ Agrp neurons is misbalanced levels of ATP to sustain membrane potential (V_m) and firing activity due to disrupted mitochondria function. To address this, we applied a patch-clamp approach to influence intracellular ATP content and its effect on neuronal activity (Liu et al., 2011). We used this indirect approach because reliable techniques to measure intracellular ATP levels in a cell-specific manner are still lacking. First, we patched Agrp neurons and, after acquiring a gigaohm seal, we analyzed these cells using perforated patch-clamp mode (Figure 6A). We then ruptured the patch membrane and switched the recording to whole-cell mode (Figure 6B). After dialyzing the intracellular content with pipette solution, the same neurons were recorded and the differences between whole-cell and perforated modes were

compared. To avoid perforation of the plasma membrane by antibiotics inside the cell after rupture of the patch membrane, we substituted amphotericin-B by high ATP (5 mM) in the pipette solution. The data described in the previous section (Figure 5) were all recorded in perforated mode with high ATP, and we have replicated those findings using amphotericin-B (Figure S4). Dialyzing the neuron with pipette solution allowed us to investigate the contribution of intracellular ATP levels for the electrical activity of control and Mfn1$^{-/-}$/Mfn2$^{-/-}$ neurons.

Agrp-Mfn1$^{-/-}$ and Agrp-Mfn2$^{-/-}$ neurons from mice fed a HFD showed decreased V_m during perforated patch clamp recording (Figure 6C, D), which is in agreement with decreased firing rate of these neurons (Figure 5B, F). Equalizing intracellular ATP levels by rupturing the patch membrane increased V_m in all groups, and differences between control and knockout cells were no longer observed (Figure 6C, D). The frequency of action potentials was also increased after establishing whole-cell recording in most of the neurons (Figure 6E–G). Both Agrp-Mfn1$^{-/-}$ and Agrp-Mfn2$^{-/-}$ neurons showed increased response to dialysis as analyzed by delta firing rate between perforated and whole-cell modes (Figure 6E, F). Additionally, most of the silent neurons recorded became active when switched from perforated to whole-cell recording (Figure 6E, F, red numbers). Overall, these data indicate that mitofusin deficiency in Agrp neurons leads to disruption in cellular ATP with consequent decreases in neuronal electrical activity. However, these neurons (even when silent) have intact cellular machinery to sustain cell activity when ATP levels are restored using dialysis (Figure 6G).

Metabolic adaptations in Agrp-Mfn1$^{-/-}$ and Agrp-Mfn2$^{-/-}$ mice

Agrp-Mfn2$^{-/-}$ female mice gained less weight when fed ad libitum normal chow diet (Figure S5). This decrease in body weight compared to littermate control mice was mainly due to decreases in fat mass, but not in lean mass and was not present in males (Figure S5). This gender difference in fat mass after subtle alteration of Agrp neuronal function was also observed after deletion of sirtuin 1 from these cells (Dietrich et al., 2010). Because many metabolic perturbations exhibit gender differences, our results point to the Agrp neurons as a possible site where these unexplained sex differences arise. We were unable to find differences in water intake, food intake, energy expenditure and activity that could justify the changes in body weight observed in Agrp-Mfn2$^{-/-}$ female mice (Figure S5). We found an increase in respiratory exchange ratio (RER) in Agrp-Mfn2$^{-/-}$ female mice compared to control animals, which indicate an increase in carbohydrate utilization related to fat acids as fuel (Figure S5). This change in RER is in agreement with previous reports showing that Agrp neurons are involved in nutrient partitioning in mice (Joly-Amado et al., 2012). In addition, Agrp-Mfn2$^{-/-}$ female mice showed improved glucose clearance during a GTT in two different cohorts of mice (Figure S6), and higher sensitivity in an ITT (Figure S6). In contrast, the changes in mitochondria observed in the analyzes of Agrp-Mfn1$^{-/-}$ mice (Figure 3) seem less critical to determine gross metabolic adaptations as we were unable to find significant changes in many parameters analyzed in these mice (Figure S5–6).

Mfn1 and Mfn2 in the Agrp neurons control metabolic response to HFD

Next, we analyzed the metabolic responses of Agrp-Mfn1$^{-/-}$ and Agrp-Mfn2$^{-/-}$ mice to a HFD. While male Agrp-Mfn1$^{-/-}$ mice did not show significant differences in body weight gain (Figure 7A), fat mass (Figure 7B) and lean mass (Figure 7C) compared to control mice fed HFD, females from the same genotype showed robust decrease in body weight (Figure 7D), mainly due to decreases in fat mass (Figure 7E) but not lean mass (Figure 7F). Both male and female mice that have the Mfn2 gene deleted in the Agrp neurons gained less weight in a HFD (Figure 7G, J). The decrease in body weight was mainly due to decrease in fat mass (Figure 7H, K), but not in lean mass (Figure 7I, L). These changes in fat mass were accompanied by decreases in circulating leptin levels (Figure S5–S7).

Agrp-Mfn1$^{-/-}$ female mice fed a HFD showed slightly decreased food intake during the dark cycle (Figure S7) compared to littermate control mice, a finding that was not observed in Agrp-Mfn2$^{-/-}$ female mice (Figure S7). The decrease in food intake in Agrp-Mfn1$^{-/-}$ mice was accompanied by a significant decrease in energy expenditure (Figure S7), without changes in global activity (Figure S7). Agrp-Mfn2$^{-/-}$ animals did not show differences in energy expenditure and activity (Figure S7). Finally, Agrp-Mfn2$^{-/-}$ male mice fed a HFD showed improved glucose profile in a GTT (Figure S7), similar to Agrp-Mfn2$^{-/-}$ female mice fed a normal chow diet (Figure S6). We were unable to find any other major differences in the other metabolic parameters analyzed (Figures S7).

Altogether, the above data indicate a critical role for mitochondria fusion controlled by Mfn1 and Mfn2 in the Agrp neurons to maintain appropriate gain in fat mass during periods of positive energy balance.

Discussion

Maintenance of energy homeostasis is critical for survival. In this process, intracellular mechanisms of energy sensing must be coupled to whole body energy balance to maintain integrative physiology of the organism. In support of this notion, here we present evidence for a critical role of mitochondrial dynamics in hunger-promoting Agrp neurons during metabolic switches.

Cell-specific mitochondrial dynamics in the melanocortin system

Most of the work on mitochondrial dynamics has been done in in vitro models. The difficulties of studying mitochondria changes in intact animals during physiological conditions preclude in-depth analyzes of mitochondrial dynamics in heterogeneous tissues, such as the brain. In addition, deep brain structures, such as the hypothalamus, are less accessible to in vivo imaging approaches adding an extra layer of difficulty to the study of such phenomena in physiological conditions. We have applied concepts of corpuscle analyzes that have been used in other disciplines for a long time (Wicksell, 1925, 1926) to estimate changes in mitochondria in the adult mice hypothalamus. These estimations of mitochondria density, size and morphology have been applied to biological systems and have been shown to be a reliable method to identify changes in mitochondria fusion and fission (Haemmerle et al., 2011; Jheng et al., 2012; Posakony et al., 1977; Rodriguez-

Navarro et al., 2010; Weibel, 1969; Weibel et al., 1966; Weibel et al., 1969). By counting mitochondria profiles, we revealed changes that occur in these organelles in specific neuronal populations of the melanocortin system in physiologically relevant conditions. These findings are of note because (1) they show a direct role of whole body energy balance in determining changes in mitochondria in discrete neuronal populations in the adult brain; and (2) they highlight the fundamental and cell-type specific role that mitochondria dynamics have in determining cellular adaptations to a changing metabolic environment. These observations open new vista on mitochondrial mechanisms that take place in distinct cell populations in support of proper behavioral and autonomic adaptations to the changing metabolic environment. Because mitochondrial changes are implicated in other physiological process, such as aging and hypoxia, we suggest that our findings have broad implications for cellular adaptations in varying physiological and pathological circumstances.

Contrary to other neuronal populations, for example the Purkinje cells in the cerebellum (Chen et al., 2007) and the dopamine cells in the midbrain (Lee et al., 2012; Pham et al., 2012), the lack of neither Mfn1 nor Mfn2 in Agrp neurons led to degeneration of neurons and/or axon fibers. These latter results unmask that mitofusins may regulate different intra-cellular processes in a cell-type specific manner making generalization on the function of specific mitofusins less compelling than thought to date.

Mfn1 and Mfn2 in Agrp neurons are involved in adaptation to positive energy balance

A main finding of this report is the observation that positive energy balance leads to mitochondria fusion in the Agrp neurons regulated by Mfn1 and Mfn2. Our data indicate that mitochondria fusion in these neurons during HFD is critical for determining weight gain and fat deposition. It is important to note that several other reports have linked the role of Agrp neurons with the regulation of fat mass (Claret et al., 2007; Dietrich et al., 2010; Joly-Amado et al., 2012; Krashes et al., 2011). Changes in fuel availability and hormonal signals are likely key players in determining mitochondria adaptation in Agrp neurons, and consequent regulation of fat mass.

Impaired mitochondria fusion silences Agrp neurons during HFD

We show here that the activity of Agrp neurons is altered during HFD, with decreases in the number of silent neurons that indicate an increase in the output of this neuronal population. Neurons are highly energy demanding cells, utilizing the majority of ATPs to maintain resting membrane potential and action potential rate (Attwell and Laughlin, 2001; Laughlin et al., 1998). Impairment of mitochondrial fusion leads to disruption of cellular energy metabolism (Bach et al., 2003; Guillet et al., 2011; Pich et al., 2005). We presented indirect evidence for altered intracellular levels of ATP in mitofusin deficient Agrp neurons during high-fat feeding that accounted for the electrical changes observed. High concentration of intracellular ATP (5 mM) was sufficient to rescue Agrp neurons from altered electrical activity. This concentration of ATP is similar to intracellular levels of ATP in highly active hypocretin neurons in the lateral hypothalamus (Liu et al., 2011).

Our data suggest that during positive energy balance (i.e., HFD exposure), mitochondria in Agrp neurons fuse to enable sustained, elevated neuronal activity to maximize storage of excess energy in fat. The decreased activity of Agrp neurons in mice with impaired mitochondria fusion was correlated with resistance of these mice to fat gain during HFD. Thus, together our observations unmasked a previously unsuspected role for mitochondria dynamics in Agrp neurons in the regulation of whole body energy balance with implications for the etiology of DIO. The effect of mitofusins was different in POMC neurons (Schneeberger et al., 2013). This remarkable outcome together with the tightly coupled relationship between the melanocortin system, feeding behavior and perypheral energy metabolism, offers the hypothalamic melanocortin system as a unique model to interrogate physiological relevance of other cell biological processes that have been identified in in vitro systems.

Experimental Procedures

Animals and diets

All mice were maintained in temperature and humidity controlled rooms, in a 12/12h light-dark cycle (lights on from 7:00AM – 7:00PM). Food and water were provided ad libitum unless otherwise stated. For the high-fat diet studies, mice were introduced to HFD when they were 9 weeks old. HFD was purchased from Research Diets (D12451). The Institutional Animal care and Use Committee from Yale University approved all procedures.

Body weight, body composition and follow-up

Mice were body weighted weekly and body composition was measured utilizing MRI (EchoMRI). After the 24th week of age, mice were bled, and in subsequent weeks were tested in a GTT and ITT. Mice were then killed for morphological or biochemical analyzes.

Electron microscopy

Mice were deeply anesthetized and perfused with saline containing heparin followed by fixative solution. Brains were post-fixed in fixative solution without gluteraldehyde (overnight at 4°C, gently shaking). Vibratome sections (50 μm) were collected in sequence, and 1:3 or 1:4 slices containing the arcuate nucleus were used for immunostaining. After primary antibody, sections were extensively washed, incubated with secondary antibody (2 h, RT), washed again, put in ABC, and developed with DAB. Sections were osmicated (15 min in 1% osmium tetroxide) and dehydrated in increasing ethanol concentrations. During the dehydration, 1% uranyl acetate was added to the 70% ethanol to enhance ultrastructural membrane contrast. Flat embedding in Durcupan followed dehydration. Ultrathin sections were cut on a Leica ultra microtome, collected on Formvar-coated single-slot grids, and analyzed with a Tecnai 12 Biotwin (FEI) electron microscope. All investigators were blinded to the experimental groups during the entire procedure.

Mitochondria and mitochondria-ER quantification

Random sections containing POMC, NPY-GFP or Agrp-LACZ cells with a visible nucleus were analyzed. A blinded investigator manually traced mitochondria profiles using ImageJ software. All cells were checked twice for consistency. Mitochondria cross-sectional area

and mitochondria aspect ratio (AR, major axis divided by minor axis, minimum value is 1.0) were calculated. AR was utilized as a shape descriptor. Probability plots were utilized to estimate changes in mitochondria size and shape and statistical differences were tested using Kolmogorov-Smirnov test. Mitochondria density was estimated by dividing the number of mitochondria profiles by the cytosolic or cellular areas. Mitochondria coverage was estimated by dividing the total area of mitochondria by the cytosolic or cellular areas. Differences in mitochondria density and coverage were tested using t-test. For mitochondria-ER interaction, a blinded investigator scored the number of mitochondria in contact with ER profiles in high magnification images (> 11,000 x). $P \leq 0.05$ was considered statistically significant.

Single-cell capture RT-PCR and ribosome profiling

Four-weeks old male NPY-GFP mice were killed at the beginning of the light cycle (9:00 AM) and the arcuate nucleus was cut in 250 μm slices (2/mouse) containing NPY-GFP neurons. Slices were transferred to incubation chamber at room temperature, and perfused with aCSF. Slices were 1-by-1 transferred to recording chambers in an electrophysiology setup and perfused with aCSF at 34°C. Cells (32 per mouse) were collected by suctioning the intracellular content utilizing glass pipettes. The tips of the glass pipettes were broken inside a new tube containing RLT buffer (75 μl containing β-mercaptoethanol, Qiagen). Samples were frozen at −80°C. RNA was extracted using Qiagen RNeasy Micro Kit (#74004). cDNA was synthetized using Qiagen Whole Transcriptome Kit (#207043). RT-PCR was performed in a Roche 480 LightCycler using Taqman probes.

For ribosome profiling, Agrp-Cre mice were bred to Rpl22 floxed mice. The protocol was in accordance to the original description of the animal model (Sanz et al., 2009) with minor modifications. Fifty days old mice (from both genders) were sacrificed and 5 hypothalami were pooled for each N. A total of N = 3–4 was used per group. After RNA isolation, we obtained approximately 25 ng of RNA per sample. Only samples with high enrichment for *agrp* and *npy* were used for further gene expression analyzes.

RT-PCR of hypothalamic punches

Female mice were sacrificed and fresh slices of the brain (2 mm thick) containing the hypothalamus were cut and put in RNA*later*™ stabilization reagent (Qiagen) for at least 2 days. Slices were removed from the solution and the arcuate nucleus was dissected under a dissection scope. Punches were put in RLT buffer and RNA was extracted using RNAeasy Mini Kit (Qiagen). cDNA was synthetized using Quantitect RT Kit (Qiagen, #205311). RT-PCR was performed as above.

Agrp neuronal projection

Brain sections were incubated in 0.2% Triton X-100 made in PB 0.1M for 30 min at room temperature. After this, sections were immediately reacted with the primary antibody. Sections were washed thoroughly in buffer and then reacted with the secondary antibody. Pictures of the paraventricular nucleus at 40× magnification were then captured by confocal microscopy. Using ImageJ software, the threshold of the black and white image was adjusted to remove all background below a user-defined intensity. Images were then

processed with the skeletonize feature. Twenty measurements of integrated density, within a fixed size polygon, were taken from each picture. The maximum integrated density for each picture was recorded and then averaged for all pictures from each brain.

Electrophysiology

Forty to fifty days old mice were used for these studies. Mice were killed at the beginning of the light cycle. For high-fat diet fed mice, animals were put on a HFD when 28 days old, and recorded at least 2 weeks later. The protocol utilized to record Agrp neurons was similar to what has been described for hypocretin neurons in the lateral hypothalamus (Liu et al., 2011) with minor modifications. All data were sampled at 3–10 kHz and filtered at 1–3 kHz with an Apple Macintosh computer using Axograph 4.9 (Molecular Devices). Electrophysiological data were analyzed with Axograph 4.9. Changes in firing rate were compared using Mann-Whitney U test. Differences in the % of silent neurons were tested using Fisher's exact test. $P \leq 0.05$ was considered statistically significant.

Statistical analyzes

Student's t test was used to compare two groups. When parametric distribution could not be assumed, non-parametric Mann-Whitney U test was used to test for statistical significance. One-tail or two-tail tests were based on pre-assumed hypothesis to be tested. Specific statistical tests are described in the sections above. $P \leq 0.05$ was considered statistically significant.

Supplementary Material

Refer to Web version on PubMed Central for supplementary material.

Acknowledgments

We thank Catiele Antunes, Marcelo R. Zimmer, Antonio Giaimo, Melissa Taylor, Ester de La Fuente, Jeremy Bober, and Klara Szigeti for support in the experiments described here. This work was supported by NIH (DP1 DK006850, R01AG040236 and P01NS062686), the American Diabetes Association, the Helmholtz Society (ICEMED) and by Conselho Nacional de Desenvolvimento Científico e Tecnológico (401476/2012-0, Brazil).

References

Andrews ZB, Liu ZW, Walllingford N, Erion DM, Borok E, Friedman JM, Tschop MH, Shanabrough M, Cline G, Shulman GI, et al. UCP2 mediates ghrelin's action on NPY/AgRP neurons by lowering free radicals. Nature. 2008; 454:846–851. [PubMed: 18668043]

Aponte Y, Atasoy D, Sternson SM. AGRP neurons are sufficient to orchestrate feeding behavior rapidly and without training. Nature neuroscience. 2011; 14:351–355.

Attwell D, Laughlin SB. An energy budget for signaling in the grey matter of the brain. Journal of cerebral blood flow and metabolism: official journal of the International Society of Cerebral Blood Flow and Metabolism. 2001; 21:1133–1145.

Bach D, Pich S, Soriano FX, Vega N, Baumgartner B, Oriola J, Daugaard JR, Lloberas J, Camps M, Zierath JR, et al. Mitofusin-2 determines mitochondrial network architecture and mitochondrial metabolism. A novel regulatory mechanism altered in obesity. The Journal of biological chemistry. 2003; 278:17190–17197. [PubMed: 12598526]

Broberger C, Johansen J, Johansson C, Schalling M, Hokfelt T. The neuropeptide Y agouti gene-related protein (AGRP) brain circuitry in normal, anorectic, and monosodium glutamate-treated

mice. Proceedings of the National Academy of Sciences of the United States of America. 1998; 95:15043–15048. [PubMed: 9844012]

Cerveny KL, Tamura Y, Zhang Z, Jensen RE, Sesaki H. Regulation of mitochondrial fusion and division. Trends Cell Biol. 2007; 17:563–569. [PubMed: 17959383]

Chen H, Detmer SA, Ewald AJ, Griffin EE, Fraser SE, Chan DC. Mitofusins Mfn1 and Mfn2 coordinately regulate mitochondrial fusion and are essential for embryonic development. The Journal of cell biology. 2003; 160:189–200. [PubMed: 12527753]

Chen H, McCaffery JM, Chan DC. Mitochondrial fusion protects against neurodegeneration in the cerebellum. Cell. 2007; 130:548–562. [PubMed: 17693261]

Chen H, Trumbauer M, Chen A, Weingarth D, Adams J, Frazier E, Shen Z, Marsh D, Feighner S, Guan X, et al. Orexigenic action of peripheral ghrelin is mediated by neuropeptide Y and agouti-related protein. Endocrinology. 2004; 145:2607–2612. [PubMed: 14962995]

Cipolat S, de Brito OM, Dal Zilio B, Scorrano L. OPA1 requires mitofusin 1 to promote mitochondrial fusion. Proceedings of the National Academy of Sciences of the United States of America. 2004; 101:15927–15932. [PubMed: 15509649]

Claret M, Smith MA, Batterham RL, Selman C, Choudhury AI, Fryer LG, Clements M, Al-Qassab H, Heffron H, Xu AW, et al. AMPK is essential for energy homeostasis regulation and glucose sensing by POMC and AgRP neurons. The Journal of clinical investigation. 2007; 117:2325–2336. [PubMed: 17671657]

Clark JT, Kalra PS, Crowley WR, Kalra SP. Neuropeptide-Y and Human Pancreatic-Polypeptide Stimulate Feeding-Behavior in Rats. Endocrinology. 1984; 115:427–429. [PubMed: 6547387]

Cone RD. Anatomy and regulation of the central melanocortin system. Nature neuroscience. 2005; 8:571–578.

Coppola A, Liu ZW, Andrews ZB, Paradis E, Roy MC, Friedman JM, Ricquier D, Richard D, Horvath TL, Gao XB, et al. A central thermogenic-like mechanism in feeding regulation: an interplay between arcuate nucleus T3 and UCP2. Cell metabolism. 2007; 5:21–33. [PubMed: 17189204]

Diano S, Liu ZW, Jeong JK, Dietrich MO, Ruan HB, Kim E, Suyama S, Kelly K, Gyengesi E, Arbiser JL, et al. Peroxisome proliferation-associated control of reactive oxygen species sets melanocortin tone and feeding in diet-induced obesity. Nature medicine. 2011; 17:1121–1127.

Dietrich M, Antunes C, Geliang G, Liu Z, Borok E, Nie Y, Xu A, Souza D, Gao Q, Diano S, et al. Agrp neurons mediate Sirt1's action on the melanocortin system and energy balance: roles for Sirt1 in neuronal firing and synaptic plasticity. The Journal of neuroscience: the official journal of the Society for Neuroscience. 2010; 30:11815–11825. [PubMed: 20810901]

Dietrich MO, Horvath TL. Feeding signals and brain circuitry. The European journal of neuroscience. 2009; 30:1688–1696. [PubMed: 19878280]

Eura Y, Ishihara N, Yokota S, Mihara K. Two mitofusin proteins, mammalian homologues of FZO, with distinct functions are both required for mitochondrial fusion. J Biochem. 2003; 134:333–344. [PubMed: 14561718]

Guillet V, Gueguen N, Cartoni R, Chevrollier A, Desquiret V, Angebault C, Amati-Bonneau P, Procaccio V, Bonneau D, Martinou JC, et al. Bioenergetic defect associated with mKATP channel opening in a mouse model carrying a mitofusin 2 mutation. FASEB journal: official publication of the Federation of American Societies for Experimental Biology. 2011; 25:1618–1627. [PubMed: 21285398]

Haemmerle G, Moustafa T, Woelkart G, Buttner S, Schmidt A, van de Weijer T, Hesselink M, Jaeger D, Kienesberger PC, Zierler K, et al. ATGL-mediated fat catabolism regulates cardiac mitochondrial function via PPAR-alpha and PGC-1. Nature medicine. 2011; 17:1076–1085.

Hahn TM, Breininger JF, Baskin DG, Schwartz MW. Coexpression of Agrp and NPY in fasting-activated hypothalamic neurons. Nature neuroscience. 1998; 1:271–272.

Horvath TL, Bechmann I, Naftolin F, Kalra SP, Leranth C. Heterogeneity in the neuropeptide Y-containing neurons of the rat arcuate nucleus: GABAergic and non-GABAergic subpopulations. Brain research. 1997; 756:283–286. [PubMed: 9187344]

Horvath TL, Sarman B, García-Cáceres C, Enriori PJ, Sotonyi P, Shanabrough M, Borok E, Argente J, Chowen JA, Perez-Tilve D, et al. Synaptic input organization of the melanocortin system predicts

diet-induced hypothalamic reactive gliosis and obesity. Proceedings of the National Academy of Sciences of the United States of America. 2010; 107:14875–14880. [PubMed: 20679202]

Horvath TL, Warden CH, Hajos M, Lombardi A, Goglia F, Diano S. Brain uncoupling protein 2: uncoupled neuronal mitochondria predict thermal synapses in homeostatic centers. Journal of Neuroscience. 1999; 19:10417–10427. [PubMed: 10575039]

Ishihara N, Eura Y, Mihara K. Mitofusin 1 and 2 play distinct roles in mitochondrial fusion reactions via GTPase activity. J Cell Sci. 2004; 117:6535–6546. [PubMed: 15572413]

Jahani-Asl A, Cheung EC, Neuspiel M, MacLaurin JG, Fortin A, Park DS, McBride HM, Slack RS. Mitofusin 2 protects cerebellar granule neurons against injury-induced cell death. The Journal of biological chemistry. 2007; 282:23788–23798. [PubMed: 17537722]

Jheng HF, Tsai PJ, Guo SM, Kuo LH, Chang CS, Su IJ, Chang CR, Tsai YS. Mitochondrial fission contributes to mitochondrial dysfunction and insulin resistance in skeletal muscle. Molecular and cellular biology. 2012; 32:309–319. [PubMed: 22083962]

Joly-Amado A, Denis RG, Castel J, Lacombe A, Cansell C, Rouch C, Kassis N, Dairou J, Cani PD, Ventura-Clapier R, et al. Hypothalamic AgRP-neurons control peripheral substrate utilization and nutrient partitioning. The EMBO journal. 2012; 31:4276–4288. [PubMed: 22990237]

Kohno D, Sone H, Minokoshi Y, Yada T. Ghrelin raises [Ca2+]i via AMPK in hypothalamic arcuate nucleus NPY neurons. Biochemical and Biophysical Research Communications. 2008; 366:388–392. [PubMed: 18068666]

Krashes MJ, Koda S, Ye C, Rogan SC, Adams AC, Cusher DS, Maratos-Flier E, Roth BL, Lowell BB. Rapid, reversible activation of AgRP neurons drives feeding behavior in mice. The Journal of clinical investigation. 2011; 121:1424–1428. [PubMed: 21364278]

Laughlin SB, de Ruyter van Steveninck RR, Anderson JC. The metabolic cost of neural information. Nature neuroscience. 1998; 1:36–41.

Lee S, Sterky FH, Mourier A, Terzioglu M, Cullheim S, Olson L, Larsson NG. Mitofusin 2 is necessary for striatal axonal projections of midbrain dopamine neurons. Human molecular genetics. 2012

Lewis MR, Lewis WH. Mitochondria in Tissue Culture. Science. 1914; 39:330–333. [PubMed: 17794648]

Liu ZW, Gan G, Suyama S, Gao XB. Intracellular energy status regulates activity in hypocretin/orexin neurones: a link between energy and behavioural states. The Journal of physiology. 2011; 589:4157–4166. [PubMed: 21727218]

Newton AJ, Hess S, Paeger L, Vogt MC, Fleming Lascano J, Nillni EA, Bruning JC, Kloppenburg P, Xu AW. AgRP Innervation onto POMC Neurons Increases with Age and Is Accelerated with Chronic High-Fat Feeding in Male Mice. Endocrinology. 2012

Ollmann MM, Wilson BD, Yang YK, Kerns JA, Chen YR, Gantz I, Barsh GS. Antagonism of central melanocortin receptors in vitro and in vivo by Agouti-related protein. Science. 1997; 278:135–138. [PubMed: 9311920]

Pham AH, Meng S, Chu QN, Chan DC. Loss of Mfn2 results in progressive, retrograde degeneration of dopaminergic neurons in the nigrostriatal circuit. Human molecular genetics. 2012

Pich S, Bach D, Briones P, Liesa M, Camps M, Testar X, Palacin M, Zorzano A. The Charcot-Marie-Tooth type 2A gene product, Mfn2, up-regulates fuel oxidation through expression of OXPHOS system. Human molecular genetics. 2005; 14:1405–1415. [PubMed: 15829499]

Pinto S, Roseberry AG, Liu H, Diano S, Shanabrough M, Cai X, Friedman JM, Horvath TL. Rapid rewiring of arcuate nucleus feeding circuits by leptin. Science. 2004; 304:110–115. [PubMed: 15064421]

Posakony JW, England JM, Attardi G. Mitochondrial growth and division during the cell cycle in HeLa cells. The Journal of cell biology. 1977; 74:468–491. [PubMed: 885911]

Reddy PH, Reddy TP, Manczak M, Calkins MJ, Shirendeb U, Mao P. Dynamin-related protein 1 and mitochondrial fragmentation in neurodegenerative diseases. Brain Res Rev. 2011; 67:103–118. [PubMed: 21145355]

Rodriguez-Navarro JA, Rodriguez L, Casarejos MJ, Solano RM, Gomez A, Perucho J, Cuervo AM, Garcia de Yebenes J, Mena MA. Trehalose ameliorates dopaminergic and tau pathology in parkin

deleted/tau overexpressing mice through autophagy activation. Neurobiology of disease. 2010; 39:423–438. [PubMed: 20546895]

Rojo M, Legros F, Chateau D, Lombes A. Membrane topology and mitochondrial targeting of mitofusins, ubiquitous mammalian homologs of the transmembrane GTPase Fzo. J Cell Sci. 2002; 115:1663–1674. [PubMed: 11950885]

Santel A, Frank S, Gaume B, Herrler M, Youle RJ, Fuller MT. Mitofusin-1 protein is a generally expressed mediator of mitochondrial fusion in mammalian cells. J Cell Sci. 2003; 116:2763–2774. [PubMed: 12759376]

Santel A, Fuller MT. Control of mitochondrial morphology by a human mitofusin. J Cell Sci. 2001; 114:867–874. [PubMed: 11181170]

Sanz E, Yang L, Su T, Morris DR, McKnight GS, Amieux PS. Cell-type-specific isolation of ribosome-associated mRNA from complex tissues. Proceedings of the National Academy of Sciences of the United States of America. 2009; 106:13939–13944. [PubMed: 19666516]

Schneeberger M, Dietrich MO, Sebastián D, Imbernón M, Castaño C, Garcia A, Esteban Y, Gonzalez-Franquesa A, Rodríguez IC, Bortolozzi A, et al. Mitofusin 2 in POMC Neurons Connects ER Stress with Leptin Resistance and Energy Imbalance. Cell. 2013

Smirnova E, Shurland DL, Ryazantsev SN, van der Bliek AM. A human dynamin-related protein controls the distribution of mitochondria. The Journal of cell biology. 1998; 143:351–358. [PubMed: 9786947]

Song Z, Ghochani M, McCaffery JM, Frey TG, Chan DC. Mitofusins and OPA1 mediate sequential steps in mitochondrial membrane fusion. Mol Biol Cell. 2009; 20:3525–3532. [PubMed: 19477917]

Sternson SM, Shepherd GMG, Friedman JM. Topographic mapping of VMH --> arcuate nucleus microcircuits and their reorganization by fasting. Nature neuroscience. 2005; 8:1356–1363.

Takahashi KA, Cone RD. Fasting induces a large, leptin-dependent increase in the intrinsic action potential frequency of orexigenic arcuate nucleus neuropeptide Y/Agouti-related protein neurons. Endocrinology. 2005; 146:1043–1047. [PubMed: 15591135]

Weibel ER. Stereological principles for morphometry in electron microscopic cytology. International review of cytology. 1969; 26:235–302. [PubMed: 4899604]

Weibel ER, Kistler GS, Scherle WF. Practical stereological methods for morphometric cytology. The Journal of cell biology. 1966; 30:23–38. [PubMed: 5338131]

Weibel ER, Staubli W, Gnagi HR, Hess FA. Correlated morphometric and biochemical studies on the liver cell. I. Morphometric model, stereologic methods, and normal morphometric data for rat liver. The Journal of cell biology. 1969; 42:68–91. [PubMed: 4891915]

Wicksell S. The Corpuscle Problem: A Mathematical Study of a Biometric Problem. Biometrika. 1925

Wicksell S. The corpuscle problem. Second memoir case of ellipsoidal corpuscles. Biometrika. 1926

Yang Y, Atasoy D, Su HH, Sternson SM. Hunger states switch a flip-flop memory circuit via a synaptic AMPK-dependent positive feedback loop. Cell. 2011; 146:992–1003. [PubMed: 21925320]

Zarjevski N, Cusin I, Vettor R, Rohner-Jeanrenaud F, Jeanrenaud B. Chronic intracerebroventricular neuropeptide-Y administration to normal rats mimics hormonal and metabolic changes of obesity. Endocrinology. 1993; 133:1753–1758. [PubMed: 8404618]

Highlights

- Mitochondria dynamics in Agrp neurons is regulated by metabolic status.
- Mitochondria fusion in Agrp neurons during HFD is dependent on Mfn1 and Mfn2.
- Impaired fusion alters the electrical activity of Agrp neurons during HFD.
- Mfn1 or Mfn2 knockout in Agrp neurons protect mice against DIO.

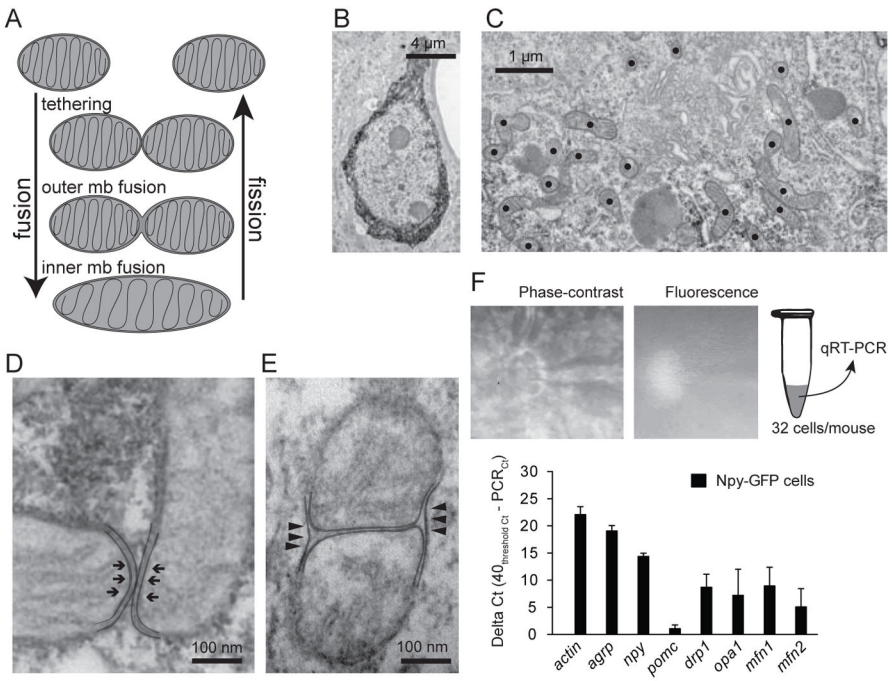

Figure 1. Mitochondria dynamics in the orexigenic Agrp neurons

(A) Mitochondria fusion and fission are multistep mechanisms that participate in mitochondria dynamics. (B) Agrp neuron labeled using immunohistochemistry and prepared for electron microscopy. (C) Labeled mitochondria profiles in a stained Agrp neuron. (D) Tethering mitochondria and (E) outer mitochondria membrane fusion in Agrp neurons. (F) NPY-GFP cells in the arcuate nucleus were captured using glass pipettes and utilized for RT-PCR of genes involved in mitochondrial dynamics (mean ± SEM). N = 32 cells/mouse, 3–4 mice/gene.

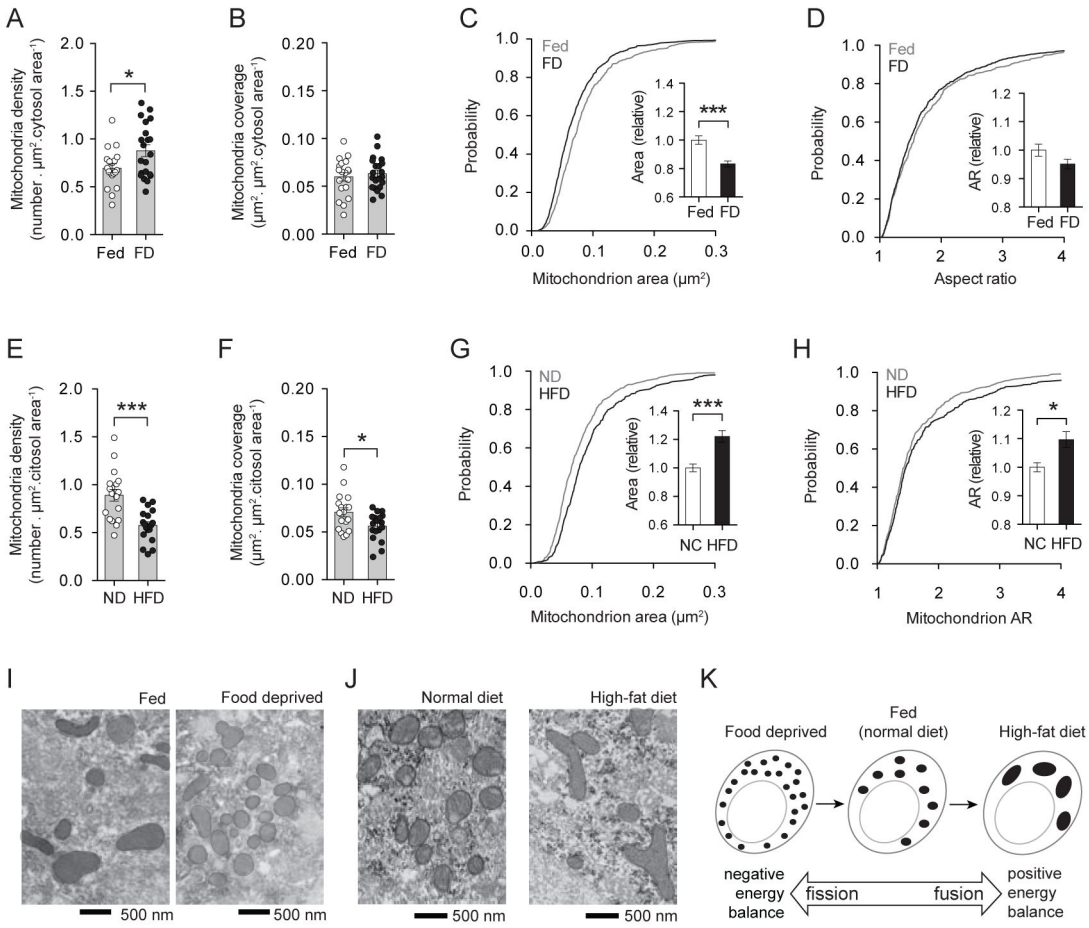

Figure 2. Mitochondria fusion-fission in Agrp neurons varies with metabolic status

(A) Mitochondria density, and (B) mitochondria coverage in Agrp neurons from fed and 24h food deprived (FD) mice. (C) Cumulative probability distribution of cross-sectional mitochondria area in Agrp neurons of fed and FD mice; insert, relative change in mean mitochondria area between fed and FD mice. (D) Cumulative probability distribution of the aspect ratio (AR) of mitochondria in Agrp neurons; insert, relative changes in mean AR between fed and FD mice. N (fed) = 527 mitochondria/19 cells/4 mice; N (FD) = 729 mitochondria/21 cells/4 mice. (E–H) Differences in mitochondria parameters between mice fed normal chow diet (ND) and a HFD similarly to (A–D). N (ND) = 629 mitochondria/18 cells/3 mice; N (HFD) = 417 mitochondria/18 cells/3 mice. (I) Representative electron micrographs of mitochondria profiles in Agrp neurons from fed and FD mice. (J) Similar to (I), mitochondria labeled in Agrp neurons of mice fed ND or a HFD. (K) Schematic showing the transition from negative energy balance to positive energy balance, and the concomitant changes in mitochondria fusion-fission. All mice were male. Bars represent mean ± SEM. Symbols represent individual values. * $P < 0.05$, *** $P < 0.001$. See also Figures S1 and S2.

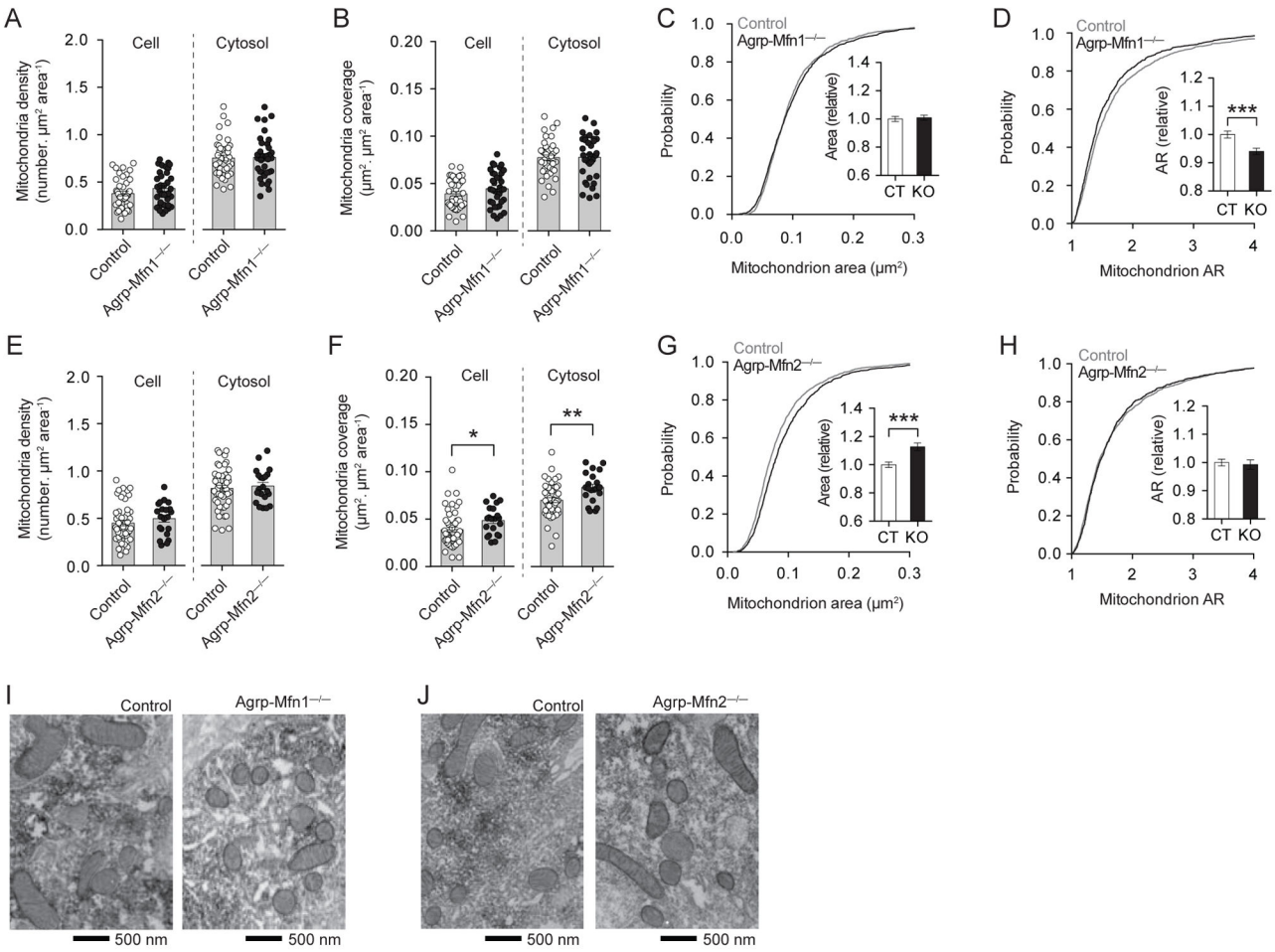

Figure 3. Role of Mfn1 and Mfn2 in mitochondria morphology in Agrp neurons from normal chow fed mice

(A) Mitochondria density, and (B) mitochondria coverage in Agrp neurons from littermate control and Agrp-Mfn1$^{-/-}$ mice. (C) Cumulative probability distribution of cross-sectional mitochondria area in Agrp neurons of control and Agrp-Mfn1$^{-/-}$ mice; insert, relative change in mean mitochondria area. (D) Cumulative probability distribution of the aspect ratio (AR) of mitochondria in Agrp neurons; insert, relative changes in mean AR. N (Control) = 1329 mitochondria/42 cells/3 mice; N (Mfn1$^{-/-}$) = 1228 mitochondria/35 cells/4 mice. (E–H) Similarly to (A–D), the data describe mitochondria density and morphology in Agrp-Mfn2$^{-/-}$ mice. N (Control) = 1565 mitochondria/49 cells/9 mice; N (Mfn2$^{-/-}$) = 728 mitochondria/21 cells/4 mice. (I–J) Representative electron micrographs of mitochondria profiles in Agrp neurons from (I) Agrp-Mfn1$^{-/-}$ mice and (J) Agrp-Mfn2$^{-/-}$ mice. Data are pooled from both male and female. Bars represent mean ± SEM. Symbols represent individual values. * P < 0.05, ** P < 0.01, *** P < 0.001. See also Figure S3.

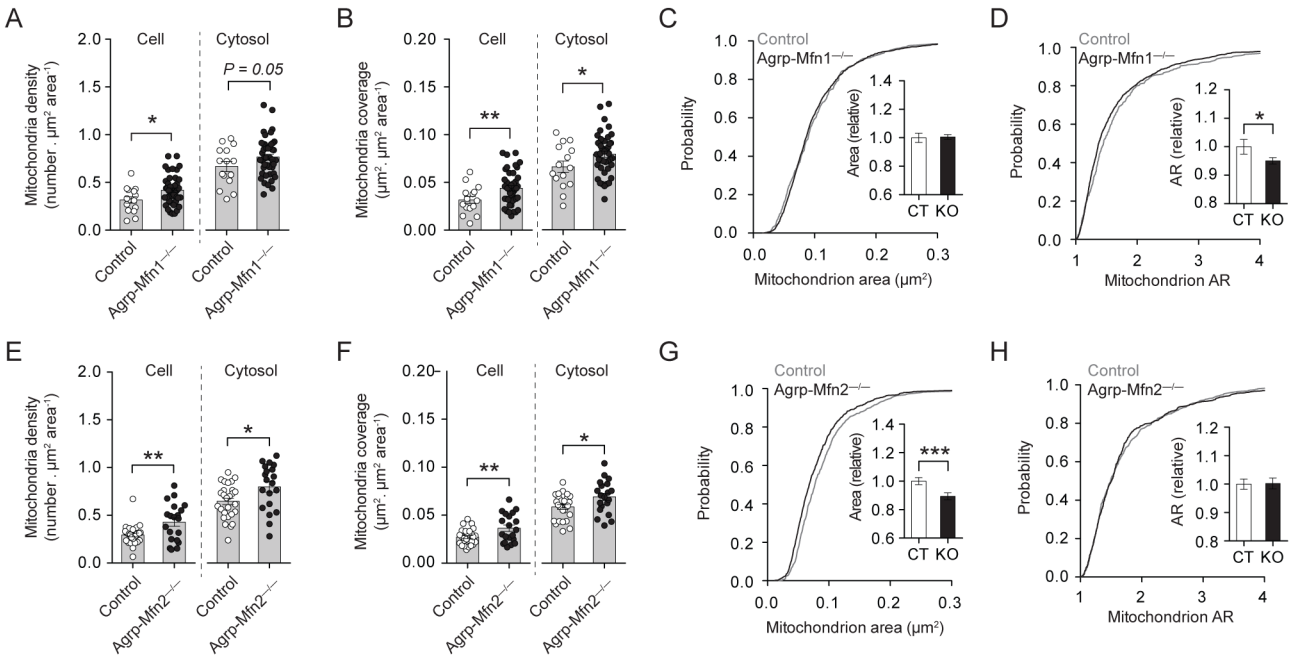

Figure 4. Mfn1 and Mfn2 in Agrp neurons critically regulate mitochondria fusion in response to high-fat diet

(A) Mitochondria density, and (B) mitochondria coverage in Agrp neurons from littermate control and Agrp-Mfn1$^{-/-}$ mice fed a HFD. (C) Cumulative probability distribution of cross-sectional mitochondria area in Agrp neurons of control and Agrp-Mfn1$^{-/-}$ mice; insert, relative change in mean mitochondria area. (D) Cumulative probability distribution of the aspect ratio (AR) of mitochondria in Agrp neurons; insert, relative changes in mean AR. N (Control) = 333 mitochondria/15 cells/3 mice; N (Mfn1$^{-/-}$) = 1363 mitochondria/44 cells/3 mice. (E–H) Similarly to (A–D), the data describe mitochondria density and morphology in Agrp-Mfn2$^{-/-}$ mice. N (Control) = 601 mitochondria/27 cells/4 mice; N (Mfn2$^{-/-}$) = 579 mitochondria/20 cells/5 mice. Data are pooled from both male and female mice. Bars represent mean ± SEM. Symbols represent individual values. * P < 0.05, ** P < 0.01, *** P < 0.001. See also Figure S3.

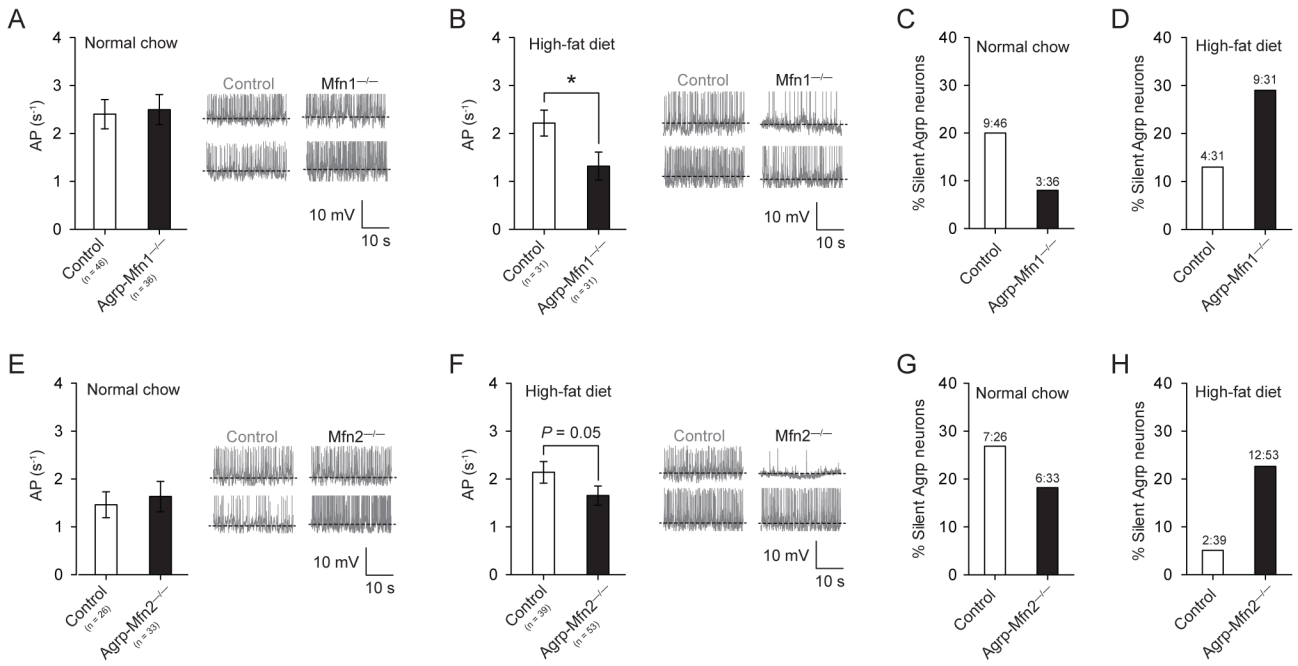

Figure 5. Mitochondria fusion regulates the electrical activity of Agrp neurons in response to high-fat feeding

(A, E) In normal chow conditions, both control and Agrp-Mfn1$^{-/-}$ or Mfn2$^{-/-}$ neurons have similar frequency of action potential (AP) as recorded using slice whole-cell recording. (B, F) When mice were fed a HFD, Agrp-Mfn1$^{-/-}$ or Mfn2$^{-/-}$ neurons have decreased AP frequency compared to control cells. (C, G) Percentage of silent Agrp neurons in control and Agrp-Mfn1$^{-/-}$ or Mfn2$^{-/-}$ mice fed a normal chow diet. (D, H) In HFD, increased percentage of silent Agrp neurons in both Agrp-Mfn1$^{-/-}$ and Agrp-Mfn2$^{-/-}$ mice compared to control mice ($P < 0.05$, Fisher's test). Data are pooled from both male and female mice. In A, B, E and F bars represent mean ± SEM. In C, D, G and H bars represent absolute values. Representative traces are plotted in panels A–B, E–F. * $P < 0.05$. See also Figure S4.

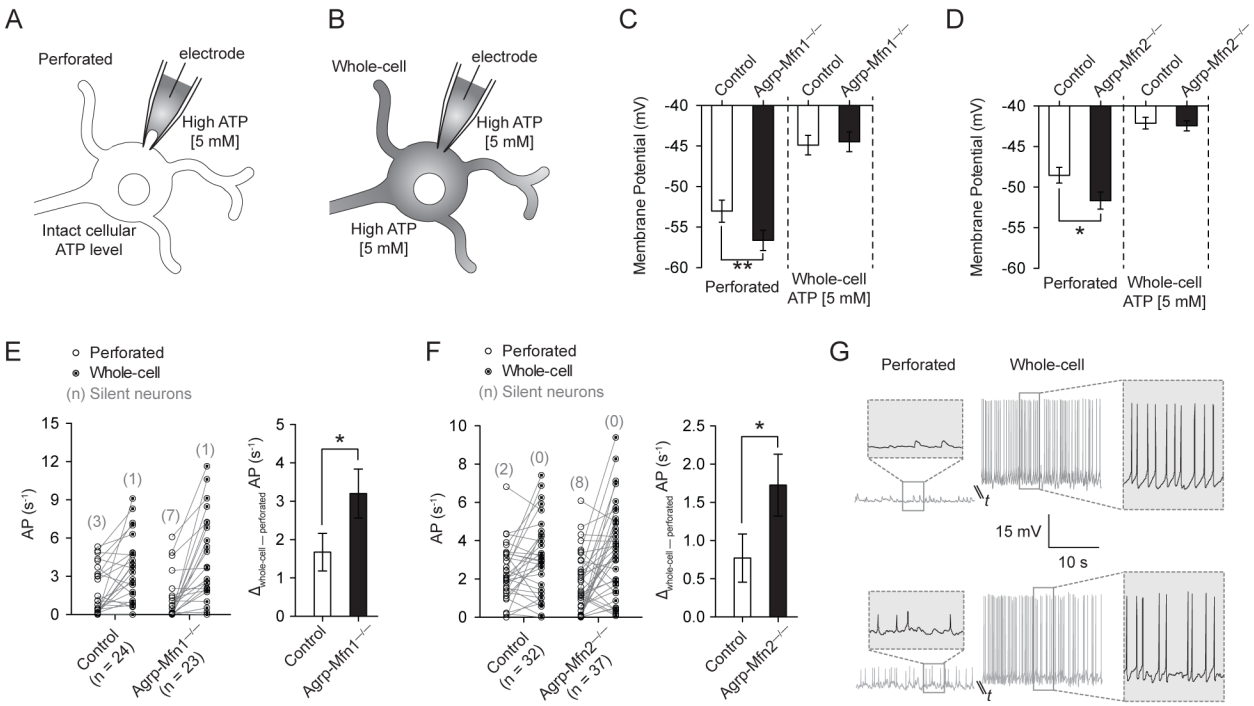

Figure 6. Intracellular ATP levels determine electrical differences in Agrp-Mfn1$^{-/-}$ and Agrp-Mfn2$^{-/-}$ neurons

(A) Schematic illustration showing patch clamp recording utilizing perforated clamp with high ATP (5 mM) in the pipette solution or (B) traditional whole-cell recording after patch membrane rupture. (C) Membrane potential in control and Agrp-Mfn1$^{-/-}$ neurons during perforated and whole-cell recordings. (D) Similar to (C), data represent recordings from control and Agrp-Mfn2$^{-/-}$ neurons. (E) Firing rate of control and Agrp-Mfn1$^{-/-}$ cells during perforated clamp and after patch rupture. Number of silent neurons is represented in parenthesis. (F) Similar to (E), data represent recordings from control and Agrp-Mfn2$^{-/-}$ neurons. (G) Two representative traces to illustrate the electrical responses of Agrp neurons during perforated and whole-cell recordings. The cell on the top is silent during perforated clamp, and becomes highly active after successful membrane rupture and whole-cell recording. Bars represent mean ± SEM. * $P < 0.05$, ** $P < 0.01$.

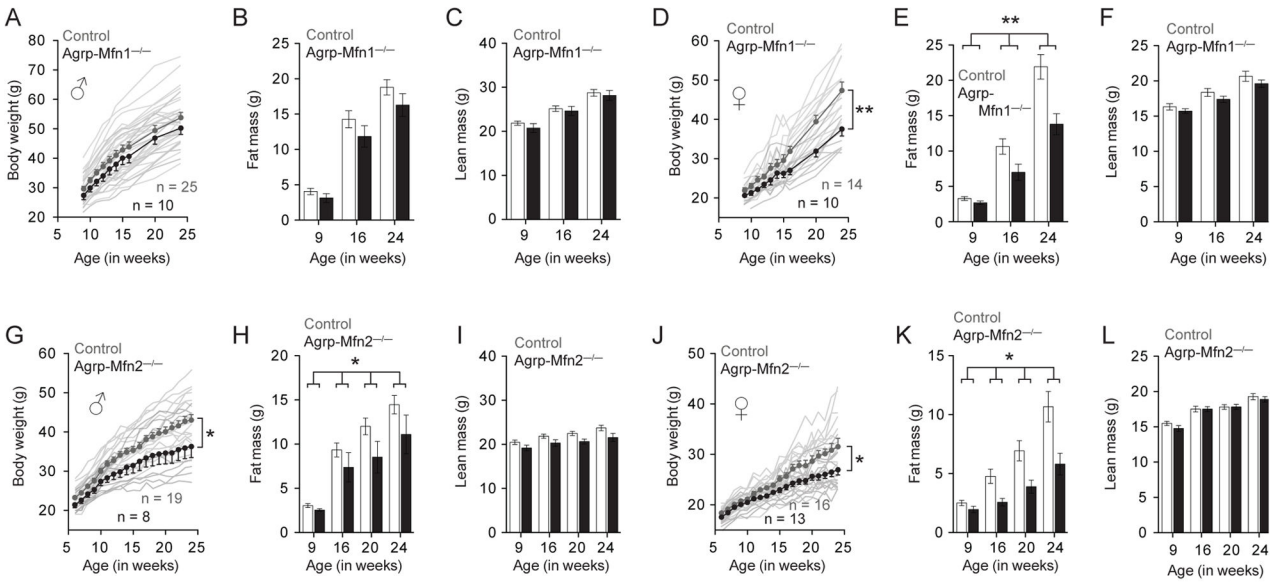

Figure 7. Metabolic response of Agrp-Mfn1$^{-/-}$ and Agrp-Mfn2$^{-/-}$ mice to diet-induced obesity

(A) Body weight curve of control and Agrp-Mfn1$^{-/-}$ male mice. (B) Fat mass and (C) lean mass in the same animals as measured by MRI. (D–F) Similar to (A–C), but data correspond to female mice. A–C, n = 25 (control) and n = 10 (Mfn1$^{-/-}$); D–F, n = 14 (control) and n = 10 (Mfn1$^{-/-}$). (G–L) Similar to (A–F), data correspond to control and Agrp-Mfn2$^{-/-}$ mice fed a HFD. G–I, n = 19 (control) and n = 8 (Mfn2$^{-/-}$); J–L, n = 16 (control) and n = 13 (Mfn2$^{-/-}$). In A, D, G and J symbols represent mean ± SEM; shadow lines represent individual mouse body weight curve. Bars represent mean ± SEM. * $P < 0.05$, ** $P < 0.01$. See also Figures S5–S7.